Geometrical Barriers in High-Temperature Superconductors

E. Zeldov,[1] A. I. Larkin,[1,2] V. B. Geshkenbein,[1,2] M. Konczykowski,[3] D. Majer,[1] B. Khaykovich,[1] V. M. Vinokur,[4] and H. Shtrikman[1]

[1]*Department of Condensed Matter Physics, The Weizmann Institute of Science, 76100 Rehovot, Israel*
[2]*L. D. Landau Institute for Theoretical Physics, 117940 Moscow, Russia*
[3]*Laboratoire des Solides Irradies, Ecole Polytechnique, 91128 Palaiseau, France*
[4]*Argonne National Laboratory, Argonne, Illinois 60439*

(Received 4 April 1994)

A theoretical description of vortex dynamics in thin flat samples is derived and is found to compare favorably with experimental results. In perpendicular applied magnetic field the vortex penetration is delayed significantly due to the presence of a potential barrier of geometrical origin. This novel geometrical barrier effect results in hysteretic magnetization and in the existence of an irreversibility line in the *absence* of bulk pinning. Among the unique characteristics of the barrier are a vortex concentration in the center of the sample and a zero-field peak in the magnetization loops.

PACS numbers: 74.60.Ec, 74.60.Ge, 74.60.Jg

The understanding of vortex dynamics in high-temperature superconductors (HTSC) is based to a large extent on the results of magnetization measurements [1]. Hysteretic magnetic behavior is usually interpreted as evidence for finite critical currents due to the bulk pinning of the vortices. Some recent experiments also suggest the existence of Bean-Livingston (BL) surface barriers [2] as a possible source of the hysteretic behavior. In this Letter we present a new theoretical derivation and experimental evidence for an additional significant source of irreversibility which we denote as the "geometrical barrier." This barrier results in hysteretic magnetization in a type-II superconductor in the *absence* of any bulk pinning of the vortices. The spatially extended Meissner current in a thin flat sample in perpendicular field results in effective trapping of the vortices in the center of the sample. The geometrical barrier is expected to dominate the observed magnetic behavior of HTSC at elevated temperatures where critical currents are relatively low. A related behavior of edge pinning was observed in type-I superconductors [3,4].

We consider a thin superconducting strip of rectangular cross section of width $2W(-W < x < W)$ and thickness d $(-d/2 < z < d/2$ and $d \ll W)$ which infinitely extends in the y direction. A perpendicular magnetic field H_a is applied along the positive z direction. In this configuration the resulting Meissner current and field profiles are given by [5,6]

$$J_y(x) = -\frac{cH_a}{2\pi d}\frac{x}{\sqrt{W^2 - x^2}}, \qquad |x| < W,$$
$$B_z(x) = \frac{H_a|x|}{\sqrt{x^2 - W^2}}, \qquad |x| > W. \tag{1}$$

In this paper we consider samples with $d \gg \lambda$ (λ is the penetration length). In this case the current flows primarily near the flat surfaces; however, in the following analysis only the current density averaged over the thickness $J_y(x)$ is of importance. The Meissner current exerts a Lorentz force on a vortex, resulting in a position-dependent vortex energy per unit length that can be approximated by $\epsilon(x) = \epsilon_0 + (\phi_0/c)\int_x^W J_y(t)dt$ not too close to the edges. ϵ_0 is the line energy of a noninteracting vortex and ϕ_0 is the flux quantum. In increasing H_a the vortices initially cut through the sharp rims of the sample without complete penetration, and thus effectively round off the curvature of the edges on the order of $d/2$. As a result, in the edge region the vortex energy increases gradually from zero to a maximum value of $\epsilon_0 d$ at $W - |x| \simeq d/2$. Clem *et al.* [3] have carried out a more complete calculation of the total Gibbs free energy in a strip with an elliptical cross section. Here we present a full solution of the current and field profiles in a rectangular strip which does not require any detailed energy considerations. The vortex potential $\epsilon(x)$, as shown in Fig. 1, is the consequence of the flat geometry and not of the precise shape of the sample edges [7]. The potential demonstrates the unique behavior of a flat sample in contrast to a thin ellipsoid where the Lorentz energy is exactly compensated by the nonuniform vortex energy due to the elliptical thickness variation [3,8]. In contrast to the BL barrier, which is very sensitive to surface quality, the geometrical barrier is very robust, since it extends over the entire sample width. In addition, there should be no appreciable thermal activation over such an extended barrier, which involves macroscopic energy $\sim \epsilon_0 d$.

The equilibrium condition for vortex penetration is obtained when the Gibbs potential in the sample center is zero, which occurs at $H_{eq} = H_{c1}d/2W$ and magnetization of $M_{eq} = H_{c1}/16$. In contrast to the elliptical cross section case, no vortices penetrate the rectangular strip at this field due to the large *macroscopic* potential barrier. Vortex penetration occurs at significantly higher applied fields when the Lorentz force, $J_y(x)\phi_0/c$, at $W - |x| \simeq d/2$ reaches the value of $2\epsilon_0/d$. From Eq. (1) the resulting penetration field is $\sim H_p = H_{c1}\sqrt{d/W}$ and $M_p \simeq (H_{c1}/8)\sqrt{W/d}$, and hence H_{c1} is overestimated by a factor

0031-9007/94/73(10)/1428(4)$06.00

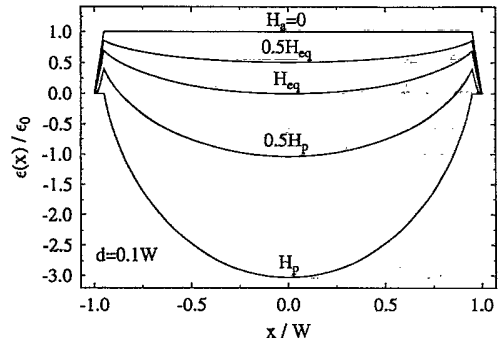

FIG. 1. Vortex potential at various applied fields $H_a \leq H_p$. At $H_a = 0$ the potential at the edges of the sample is assumed to drop linearly for simplicity.

of about $\sqrt{W/d}$ if obtained from the measured penetration field scaled by the standard elliptical demagnetization factor. Note that despite the large differences in H_p, the edge field in both cases is H_{c1} since $H_E \simeq (2W/d)H_a$ for an ellipse and $H_E \simeq H_a\sqrt{W/d}$ in a strip [4,9].

At $H_a < H_p$ vortices enter only into the edge regions at $|x| > W - d/2$. In a steady state situation we have to cut off the diverging Meissner currents at a value on the order of $J_E^0 = 2c\epsilon_0/\phi_0 d = cH_{c1}/2\pi d$ in order to balance the net force on the edge vortices. For $H_a > H_p$ there is no longer a potential barrier for vortex penetration and the Meissner currents drive the entering vortices to the center of the sample. We first analyze the case of zero bulk critical current, $J_c = 0$.

In the absence of pinning, no net current may flow in a vortex-filled region in a steady state $[|B_z(x)| > 0, J_y(x) = 0]$, and similarly, no vortices may be present in the regions of finite Meissner current $[|J_y(x)| > 0, B_z(x) = 0]$. The field components B_z and B_x outside the sample must be respectively the real and imaginary parts of an analytic function $F(s)$ of a complex variable $s = x + iz$. Since on the surface of the sample $B_x(x) = (2\pi d/c)J_y(x)$, $F(x)$ must be purely real in the vortex-filled regions and purely imaginary in the vortex-free region. A function that satisfies the above requirements is $F(s) \propto \sqrt{(b^2 - s^2)/(W^2 - s^2)}$, which results in

$$J_y(x) = 0,\ B_z(x) = H_a\sqrt{\frac{b^2 - x^2}{W^2 - x^2}},$$

at $|x| < b$ or $|x| > W$ and

$$J_y(x) = -\frac{x}{|x|}\frac{cH_a}{2\pi d}\sqrt{\frac{x^2 - b^2}{W^2 - x^2}},\ B_z(x) = 0,$$

at $b < |x| < W$, where $2b$ is the width of the vortex-filled region in the center of the strip. The procedure can readily be extended to account for the presence of an additional transport current by replacing $b^2 - s^2$ by $(b_R - s)(b_L + s)$, and will be considered elsewhere. The above solution is self-consistent for any value of b, and therefore b has to be determined from the following force-balance consideration. As the field is increased, additional vortices penetrate and expand the vortex-filled region. At any given field a steady state is reached when $|J_y(W - d/2)| = J_E^0$. From the above equation we obtain $b \simeq W\sqrt{1 - (H_p/H_a)^2}$ in the case of $d \ll W$, and the corresponding magnetization is given by $M \simeq H_a(W^2 - b^2)/8Wd = H_{c1}^2/8H_a$. The resulting current and field profiles are shown in Figs. 2(a) and 2(b). Note that the gradient in the vortex density in the central region is accompanied by vortex curvature such that $\nabla \times B = 0$. As the field increases, new vortices enter the sample and accumulate in the center. This process, however, is not reversible; if the field is decreased, the vortices remain trapped by the Meissner currents, and the width of the vortex-filled region increases, maintaining constant trapped flux in the central region. Vortices leave the sample only when b reaches $W - d/2$. A reversible situation is obtained at fields on the order of H_{c1} when the vortex-filled region fills the entire sample. J_E^0 continues to flow at the edges and results in reversible magnetization of $\sim H_{c1}/4\pi$. Hence, in the *absence* of pinning the geometrical barrier results in hysteretic magnetization and in an irreversibility line that follows the temperature dependence of H_{c1}.

In the presence of bulk pinning, the initial penetrating vortices do not reach the center of the sample, and stop at $|x| = b_p$, where the Meissner current density equals the critical current density J_c. As the field increases, vortices form two isolated vortex-filled regions at $a < |x| < b$. The central region, $|x| < a$, remains vortex-free, since $J_y(x) < J_c$ there, and no vortices can penetrate; in the outer $|x| > b$ regions $J_y(x) > J_c$, and no vortices may remain there in a steady state. Note that a significant part of the strip carries supercritical current densities which may exceed J_c significantly. For a typical HTSC monocrystal of 10 μm thickness and $H_{c1} \simeq 300$ Oe we obtain $J_E^0 \simeq 5 \times 10^4$ A/cm^2, and in a thin film of $d < 0.5$ μm the resulting J_E^0 is in excess of 10^6 A/cm^2. Since these edge currents are comparable to state-of-the-art critical currents in HTSC at elevated temperatures, the geometrical barrier is a very significant effect with

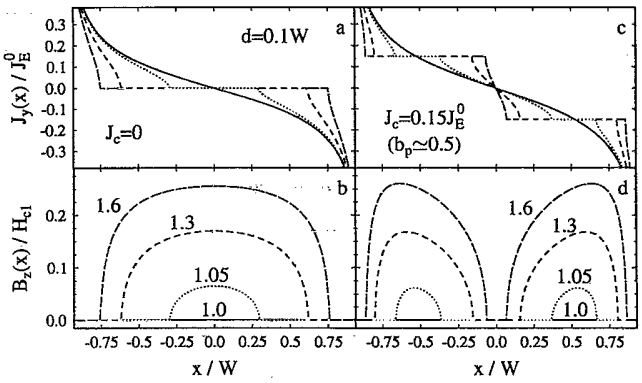

FIG. 2. The current and field profiles at indicated values of H_a/H_p for $J_c = 0$ [(a) and (b)] and $J_c = 0.15J_E^0$ [(c) and (d)] showing vortex accumulation inside the sample.

important practical implications. Note that in the presence of bulk pinning, the edge current required for vortex penetration increases, $J_E \simeq J_c + J_E^0$, since the Lorentz force at $|x| = W - d/2$ has to overcome both the pinning force and the gain in vortex potential in the edge region. In addition, J_E increases significantly when the image forces of the BL type become important. Our results can be readily extended to include this effect by replacing H_{c1} in the J_E^0 and H_p expressions with H_s, the BL surface barrier penetration field.

To derive the current and field distributions at finite J_c we resort again to complex function analysis. The procedure is similar to the $J_c = 0$ case described above and results in $F(s) = \sqrt{(s^2 - a^2)(b^2 - s^2)/(e^2 - s^2)}$, where $0 \le a \le b \le W - d/2 \le e \le W$. However, the requirement for the current in the vortex-filled regions $a < |x| < b$ is now $|J_y(x)| = J_c$, rather than $J_y(x) = 0$, and we also include here a rigorous current limitation at the edges, $J_y(x) = J_E$ at $e < |x| < W$. This is achieved by multiplying $F(s)$ by $f(s)$ such that $\mathrm{Im}\{f(x)\} = 0$ everywhere except at $a < |x| < b$, where we require $\mathrm{Im}\{f(x)\} = 1/F(x)$, and $\mathrm{Im}\{f(x)\} = 1/\gamma F(x)$ at $e < |x| < W$ ($\gamma = J_c/J_E$). As a result

$$J_y(x) = \begin{cases} -J_c f(x)\sqrt{\frac{(a^2-x^2)(b^2-x^2)}{(e^2-x^2)}}, & 0 < x < a \\ & \text{or } b < x < e, \\ -J_c, & a < x < b, \\ -J_E, & e < x < W, \end{cases}$$

and $-J_y(|x|)$ for $x < 0$, and

$$B_z(x) = \begin{cases} 0, & |x| < a \quad \text{or} \quad b < |x| < e, \\ \frac{2\pi J_c d}{c}\,\mathrm{Re}\{f(x)\}\sqrt{\frac{(x^2-a^2)(b^2-x^2)}{(e^2-x^2)}}, & \\ & a < |x| < b \quad \text{or} \quad |x| > e. \end{cases}$$

$\mathrm{Re}\{f(x)\}$ is given by the Cauchy integral

$$\mathrm{Re}\{f(x)\} = \frac{2x}{\pi}\left[\mathrm{P}\int_a^b \frac{dt/\mathrm{Im}\{F(t)\}}{x^2 - t^2} + \frac{1}{\gamma}\mathrm{P}\int_e^W \frac{dt/\mathrm{Im}\{F(t)\}}{x^2 - t^2}\right].$$

The constraints on a and b are given by $B_z(\infty) = H_a$ and $f(e) = 0$ in order to provide a continuous solution at $|x| = e$; we take $e = W - d/2$ for increasing $H_a > H_p$. The above elliptic integrals are readily evaluated numerically and the resulting distributions are shown in Figs. 2(c) and 2(d). As the applied field is increased, a decreases and b increases, so that the vortex-filled regions expand rather symmetrically in both directions at moderate critical currents corresponding to $b_p \simeq 0.5$. In the low J_c limit, the two vortex-filled regions merge rapidly, and the process continues similarly to the zero critical current case. In the strong pinning case, $J_c \gg J_E^0$, the vortex-filled regions expand only inward and the results for the critical state behavior in a thin strip are recovered [5,9,10].

An additional important effect of the geometrical barrier is the strong "zero-field peak" in the magnetization loop which is routinely observed in HTSC [1]. As the field decreases from sufficiently high values, $a \simeq 0$ and $J_y(x) = \pm J_c$ in the entire sample except close to the edges. We therefore may simplify the above equations by removing the $a^2 - x^2$ terms and obtain

$$J_y(x) = \begin{cases} J_c, & 0 < x < b, \\ \frac{2J_c}{\pi}\arctan\frac{b}{e}\sqrt{\frac{e^2-x^2}{x^2-b^2}} & \\ \quad + \frac{2J_E}{\pi}\arctan\sqrt{\frac{(W^2-e^2)(x^2-b^2)}{(W^2-b^2)(e^2-x^2)}}, & b < x < e, \\ J_E, & e < x < W, \end{cases}$$

and $-J_y(x)$ for $x < 0$. The corresponding applied field and magnetization are given by

$$H_a = \frac{2H_{c1}\gamma_0}{\pi}\left[\ln\sqrt{\frac{e+b}{e-b}} - \left(1 \mp \frac{1}{\gamma_0}\right) \times \ln\frac{\sqrt{W^2 - b^2} + \sqrt{W^2 - e^2}}{\sqrt{e^2 - b^2}}\right],$$

$$M = \frac{H_{c1}\gamma_0}{4\pi W d}\left[be + \left(1 \mp \frac{1}{\gamma_0}\right)\sqrt{(W^2 - b^2)(W^2 - e^2)}\right],$$

where $\gamma_0 = J_c/J_E^0$. At high positive fields $b = e = W - d/2$, and the edge current is $J_E = J_c - J_E^0 = J_c(1 - 1/\gamma_0)$ because J_E^0 is a reversible current which has the same polarity for both ascending and descending field in contrast to J_c [11]. J_E^0 changes direction as the polarity of the edge vortices changes. As the field decreases, $b = W - d/2$, while e increases until $e = W$. At this point the applied field is still positive and substantial, $H_r \simeq (2J_c d/c)\ln(4W/d)$; however, the edge field is zero and becomes negative as $H_a < H_r$, and hence $J_E = J_c(1 + 1/\gamma_0)$. A unique situation occurs; negative vortices cannot penetrate into the sample as long as $J_y(W - d/2) < J_c + J_E^0$, but the current cannot rise

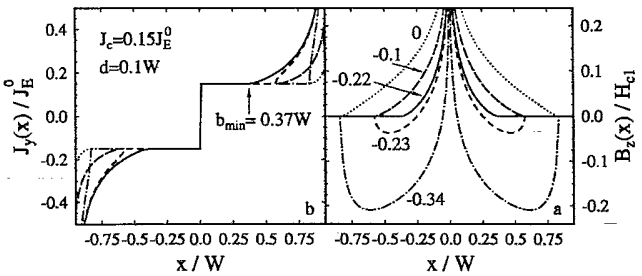

FIG. 3. The current (a) and field (b) profiles in decreasing H_a. At H_a/H_{c1} of 0, −0.1, and −0.22, positive vortices are removed from the sample; at lower fields, negative vortices start to penetrate. Maximum magnetization is obtained at $H_a/H_{c1} = -0.22$.

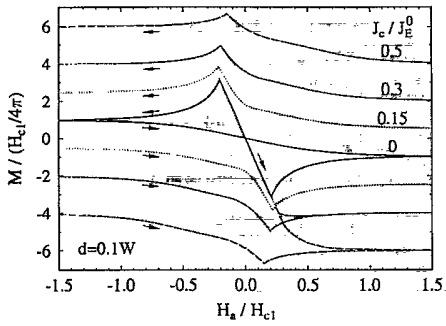

FIG. 4. Calculated full magnetization loops for various values of J_c showing the zero-field peak and the irreversible magnetization at $J_c = 0$.

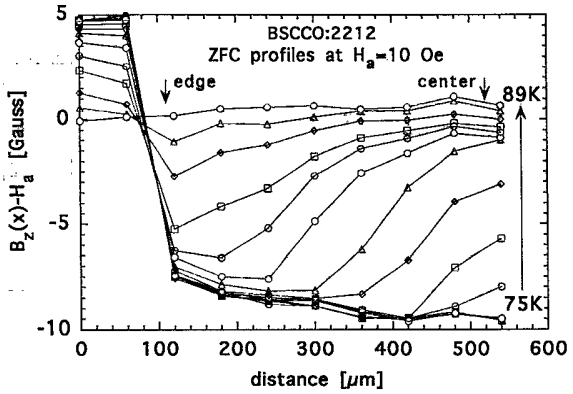

FIG. 5. Experimental field profiles in $Bi_2Sr_2CaCu_2O_8$ single crystal at various temperatures with 1 K increment. As the temperature increases, additional vortices penetrate and expand the vortex-filled region in the center of the sample.

above J_c as long as the positive vortices are present. As a result, new vortex-free regions nucleate at the edges and grow into the sample, characterized by a gradual decrease of b and e and the condition $dJ_y/dx = 0$ at $x = b$. This process is accompanied by a significant increase in the current density and the magnetization. Figure 3 shows the resulting current and field profiles, and the magnetization loops for various J_c values are shown in Fig. 4. The vortex-cleaning process continues up to negative field values on the order of $-H_p$ where the maximum magnetization is achieved when $b = b_{\min} = W/\sqrt{1 + (W^2/e^2 - 1)/\gamma^2}$ and $e = W - d/2$. As the field decreases further, the negative vortices penetrate into the sample and annihilate the remaining positive ones, and the magnetization decreases. This zero-field peak in the magnetization may be further significantly enhanced in the presence of BL barriers.

We have used novel sensitive GaAs/AlGaAs 2DEG Hall-sensor arrays to study vortex penetration and dynamics in $Bi_2Sr_2CaCu_2O_8$ single crystals. The sensor arrays of up to 11 elements were in direct contact with the crystal surface, so that $B_z(x)$ was directly measured. Sensors of various active areas in the range of 3.5×3.5 μm^2 to 50×50 μm^2 with sensitivity better than 0.1 G were used, and several various crystals were investigated. The observed vortex behavior is in very good agreement with the above derivations and will be discussed in detail elsewhere. Here we present only the unique observation of vortex penetration and accumulation in the center of the sample. Figure 5 shows the measured $B_z(x)$ profiles as the sample is gradually heated after a field of 10 G has been applied at low temperatures. As $T_c = 90$ K is approached, H_{c1} and H_p decrease, allowing more vortices to penetrate at a constant applied field [12]. Very similar behavior is observed at a constant temperature as the applied field is increased, in striking agreement with the calculated profiles in Fig. 2(b). This behavior is a direct consequence of the geometrical barrier in thin flat samples.

In conclusion, we have derived analytical solutions of a new geometrical barrier which governs vortex penetration and dynamics in flat samples of type-II superconductors in perpendicular field. The effect was observed experimentally in $Bi_2Sr_2CaCu_2O_8$ crystals using microscopic Hall-sensor arrays. The geometrical barrier results in retarded vortex penetration, vortex accumulation in the center of the sample, zero-field peak in the magnetization, and irreversible magnetization loops. The described effects of the geometrical barrier are enhanced significantly in the presence of Bean-Livingston surface barriers.

We are grateful to N. Motohira for providing the BSCCO crystals and E. Z. is grateful to John R. Clem for helpful discussions. This work was supported by the Israeli Ministry of Science and the Arts, by the Philip M. Klutznick Fund, by MINERVA foundation, and by France-Israel cooperation program PICS 112. V. M. V. acknowledges the support through U.S. Department of Energy, BES-Materials Sciences, under Contract No. W-31-109-ENG-38.

[1] For review see S. Senoussi, J. Phys. III (France) **2**, 1041 (1992); G. Blatter, M. V. Feigelman, V. B. Geshkenbein, A. I. Larkin, and V. M. Vinokur (to be published).
[2] M. Konczykowski, L. I. Burlachkov, Y. Yeshurun, and F. Holtzberg, Phys. Rev. B **43**, 13 707 (1991); C. P. Bean and J. D. Livingston, Phys. Rev. Lett. **12**, 14 (1964).
[3] J. R. Clem *et al.*, J. Low Temp. Phys. **12**, 449 (1973).
[4] J. Provost *et al.*, J. Phys. F **4**, 439 (1974).
[5] A. I. Larkin and Yu. N. Ovchinnikov, Zh. Eksp. Teor. Fiz. **61**, 1221 (1971) [Sov. Phys. JETP **34**, 651 (1972)].
[6] R. P. Huebener, R. T. Kampwirth, and J. R. Clem, J. Low Temp. Phys **6**, 275 (1972).
[7] M. V. Indenbom and E. H. Brandt (to be published).
[8] M. V. Indenbom, H. Kronmuller, T. W. Li, P. H. Kes, and A. A. Menovsky, Physica C (to be published).
[9] E. Zeldov, J. R. Clem, M. McElfresh, and M. Darwin, Phys. Rev. B **49**, 9802 (1994).
[10] E. H. Brandt and M. V. Indenbom, Phys. Rev. B **48**, 12 893 (1993).
[11] B. Khaykovich, E. Zeldov, M. Konczykowski, D. Majer, A. I. Larkin, and J. R. Clem, Physica C (to be published).
[12] Similar behavior was recently observed in Ref. [8].